X-Ray Photoelectron Spectroscopy

M12. Lucía Navarro, Pablo Hernández López

January 2019

1 Introduction

In this experiment we will perform X-ray photoelectron spectroscopy, which will allow us to study the elemental composition of a sample by the knowledge of the electronic structure of those elements. Through the energy and momentum of photoelectrons one can have information about the arrangement of electronic levels in solids, molecules or atoms.

2 Theoretical concepts

On X-ray Photoelectron Spectroscopy (XPS) the surface of a sample is illuminated with highly energetic photons (in the range of the keV), to induce the photoelectric effect. By measuring the energies of the electrons emitted one can determined the energies that kept them bound to their atoms and thus the electronic configuration of the probe.

2.1 Photoemission

The fundamental principle behind this experiment is the emission of an electron from a solid after being excited by an incident photon (photoelectron emission). In this process the photon transfers all its energy to an electron in a bound state, and if it is enough for the electron to overcome its binding energy and the work function of the solid, then the electron can be emitted. In this case the energy balance would be

$$E + h\nu = E' + E_{kin} + \Phi \tag{1}$$

where E, E' are the initial atom energy and that of the ionized atom after the electron is gone, $h\nu$ is the energy of the incident photon, E_{kin} is the kinetic energy of the photoelectron emitted and Φ is the work function of the solid. What we can measure at the laboratory by the means that will be explained later is the electron's kinetic energy:

$$E_{kin} = h\nu - (E' - E) - \Phi = h\nu - E_B - \Phi \tag{2}$$

where E_B is the binding energy related to the Fermi level (see Figure 1). Knowing the incident photon's energy we can obtain the binding energy for the emitted electrons that satisfy $E_B < h\nu$.

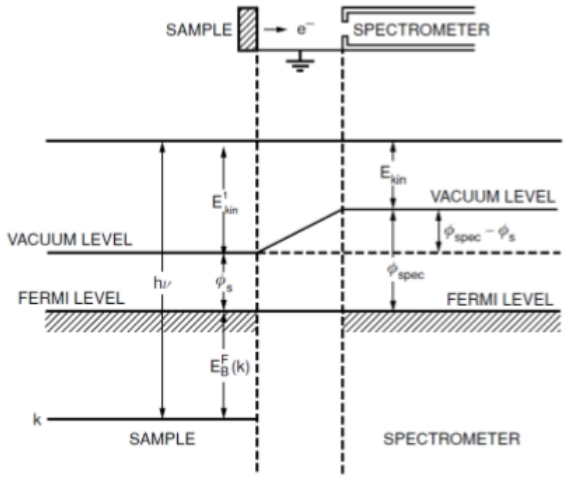

Figure 1: Scheme of the energy bands and energy differences involved in the emission of a photoelectron and the measurement of the electron's energy. To the left hand of the figure we can see the energy level structure of the sample. An electron absorbs the energy of the incident photon ($h\nu$) and has to overcome the binding energy relative to the Fermi level and the work function to leave the metal with a certain kinetic energy. This electron has then to overcome the difference between the work functions of the spectrometer and the sample to be detected.

As we can see in Figure 1, the position of the energy bands is usually referred to the Fermi level, for which the energy value E_f can be calculated as:

$$E_{kin} = E_f - E_B = h\nu - \Phi \tag{3}$$

By measuring the binding energies of the electrons in the atoms of a certain substance one can obtain very important information about its electronic configuration.

The interaction of a photon with the sample include many processes with their characteristic energies: Auger emission, emission from core levels, emission from valence band, secondary electron excitation and energy losses from inelastic scattering with electrons.

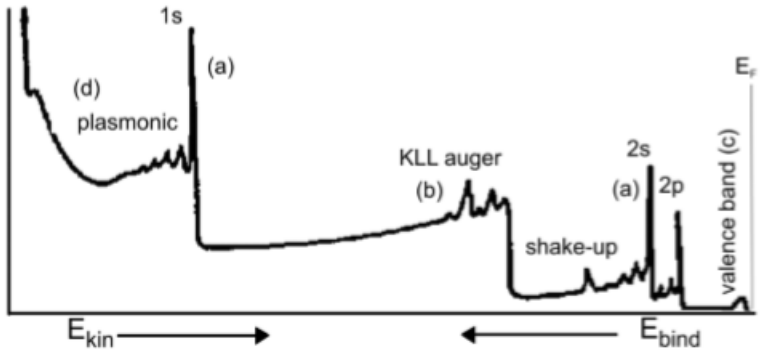

Figure 2: Example of a photoelectron spectrum. The main peaks for a spectrum of this type can be seen, as well as secondary lines such as shake-up or satellite peaks.

More lines can be observed besides the main ones, separated a certain energy distance from them, like satellite peaks from plasmon excitation, or shake-up peaks from the two-electron processes, where the emitted electron excites a second electron which is normally at a higher shell.

2.2 Binding energy

The binding energy of the electron depends on several terms which are presented in equation (3):

$$E_B = E_B^{(atom)} + \Delta E_{chem} + \Delta E_{Mad} + \Delta E_{rel} \tag{4}$$

where the additional terms can be treated as residual terms and will result in multiplet structures for the atomic levels. The chemical shift ΔE_{chem} is the additional chemical bond given by the surrounding atoms, the Madelung constant ΔE_{Mad} refers to the electrostatic energy of the solid lattice, and the relaxation term ΔE_{rel} describes the many body effects in the final state of the excited atom.

2.3 Linewidth and multiple peaks

The energy splittings of the electronic levels that we will encounter are due to two different effects: the L-S coupling and the magnetic exchange spin-spin splitting.

In the L-S coupling the orbital angular momentum of an electron l interacts with its spin s. This effect is described by the spin-orbit Hamiltonian term

$$H_{s-o} = al \cdot s \tag{5}$$

Due to this effect, the energy levels of an atom split into a doublet $l - \frac{1}{2}$, $l + \frac{1}{2}$ that can be found in the spectrum, as the emission line of a full atomic shell also splits in the same way. According to the $l \cdot s$ coupling, electrons at the s-states are not affected by this energy splitting because of their null orbital angular momentum.

On the other hand, another different kind of coupling may split our peak in two: the magnetic spin-spin exchange splitting. When considering an atom with a partially filled shell such as the 4f shell of samarium, the magnetic moment of this shell interacts with a full s shell (which in principle would not show energy splitting) by exchange coupling, causing the energy split of the two electrons in the s shell.

2.4 Surface sensitivity

In the photoelectron spectroscopy surface-sensitive measurements can be performed, where the mean free path (or mean escape depth) is a very important parameter. In fact, XPS is a very surface-sensitive technique for electron kinetic energies from 20 to 100 eV.

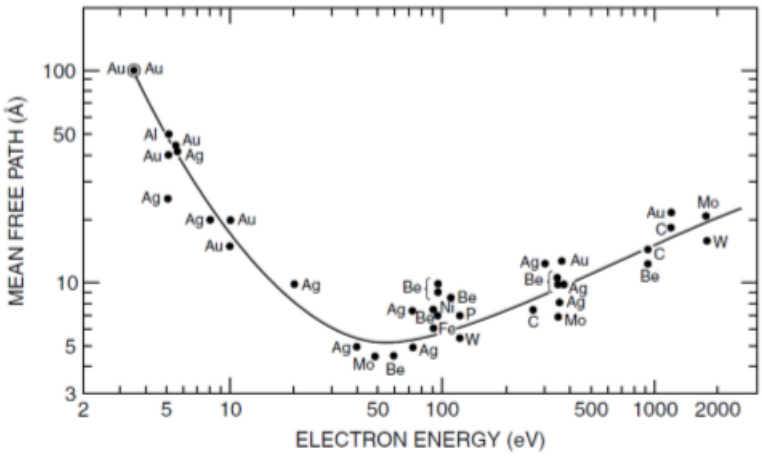

Figure 3: Universal curve of the mean free path of an electron in a solid as a function of the kinetic energy.

The surface sensitivity at XPS also depends on the incident angle of the X-ray photons, but we will not study that dependence in this report. In this experiment we will be able to do this type of measurements up to one atomic layer, as the kinetic energy of the photoelectrons can be controlled with changes in the experimental setup, as we will see in section 3.

3 Instruments

The experimental equipment needed for a X-ray photoelectron spectroscopy is the following: an UHV (ultra-high vacuum) chamber, an x-ray source, an electron energy analyzer and an evaporator. We will now make some brief remarks on these devices.

3.1 Ultra high vacuum chamber

Ultra-high vacuum (UHV) is needed to perform x-ray photoelectron spectroscopy to avoid the formation of a layer of adsorbed gas molecules on the surface of our sample, for this would alter our results because of the high surface sensitivity of this method. We will use a UHV chamber to keep our sample as clean as possible in pressures of the order of up to 10^{-11} mbar. It uses a turbo molecular pump to get a first rough vacuum of 10^{-9} mbar pumping out the heavy gases in the chamber and then a heating system to get rid of the water particles clung to the steel walls. An UHV chamber contains our Ag and Sm samples.

3.2 X-ray source

The x-ray source employed in our experiment emits the characteristic x-ray lines of the spectra of aluminum or magnesium as a radiation with a well-defined energy. Table 1 shows these characteristic energies and their line width. It consist of a cathode that emits thermal electrons when heated and an anode of one of the two aforementioned materials where the electrons impact after being accelerated. The radiation resulting of the impact of the electrons in the anode is then filtered by an aluminum window so other unwanted radiation such as bremsstrahlung is absorbed.

X-ray line	Energy [eV]	Line width [eV]
$Mg - K_\alpha$	1253.6	0.7
$Al - K_\alpha$	1486.6	0.86

Table 1. Characteristic x-lines used by our x-ray source during the experiment. K_α denotes in spectroscopic notation the x-rays produced by transitions from the n=2 to n=1 levels

3.3 Electron energy analyzer

The electron energy analyzer collects the electrons expelled from the sample and measures their kinetic energy converting the amplified signal to a measurable pulse which is the input of an electronic circuit. The electrons coming out of the sample are directed to the channneltron through a system of electrical lenses and two hemispherical metallic plates that select the electrons with a kinetic energy greater then a certain threshold value (E_{pas}) through a potential difference. This way we can filter out the low kinetic energy electrons introduced by secondary processes. Finally the electrons are multiplied in the channeltron by secondary emission in the walls of the device. Secondary emission is the physical phenomenon where primary incident electrons (or other particles) of sufficient energy hit the surface of a certain material (a dynode) or pass through it and induce the emission of secondary electrons. Thus the signal is amplified by a cascaded dynode chain where each primary electron produces multiple secondary ones.

3.4 Evaporator

Lastly the evaporator will turn the samarium stored in a crucible into its gaseous form through a heat source (a filament around this crucible) so it can be dosed in a sheet of steel and be adsorbed by it.

4 Procedure

With this experimental setup we have performed different XPS measurements. We have obtained the kinetic energy spectra of the photoelectrons of two different samples of silver (Ag) and samarium (Sm), and compared the peaks that we could find to the ones expected by the theory.

In order to obtain the spectra and accurately measure the positions of the peaks we first took a full spectrum of the samples, and by looking at the table of binding energies [3] and using Equation 2 we calculated a first rough estimation of where we expected to find the different l-s multiplets. Then we set the range and step of the spectroscopy for each group of peaks to achieve better resolution. We proceeded analogously to investigate the compounds of a 10DM coin.

4.1 Probe of a silver sample

We begun with the probing of the silver surface. After having turned on all the experimental equipment described in Section 3 and having let it warm up we adjusted the position of the sample and carried on the measurements. The spectrometer was already calibrated for the silver sample, so one was able to read the kinetic energies directly from the spectrum (without subtracting any work function).

Silver has an electronic configuration of $[Be]3s^2 3p^6 3d^{10} 4s^2 4p^6$. We obtained the spectra for the kinetic energies corresponding to the 3s, 3p and 3d subshells. As it has already been explained we first estimated where we expected to find the peaks before taking the detailed spectrum. With the literature values of the corresponding binding energies [3], we calculated the values shown in Table 2.

Level	Al source ($h\nu$=1483.6 eV)	Mg source ($h\nu$=1253.6 eV)
$3d_{3/2}, 3d_{5/2}$	1105.6 eV, 1112.6 eV	877.6 eV, 884.6 eV
$3p_{1/2}, 3p_{3/2}$	908.6 eV, 977.6 eV	651.6 eV, 680.6 eV
$3s$	761.6 eV	533.6 eV

Table 2: Energy peak positions expected for our Ag sample, for both Al and Mg X-ray sources, according to the literature values of the corresponding binding energies and considering ls coupling[3].

4.2 Probe of a samarium sample

Afterwards we probed a surface of freshly evaporated samarium. The evaporation time was around an hour. The electron energy analyzer was calibrated to take into account the work function of Ag, so we had to adjust our results for the Sm sample by measuring its Fermi level. With that value we will be able to correctly measure the energies observed in the Sm spectrum.

Samarium has the following electronic configuration: $[Xe]6s^2 4f^6$. Firstly we have obtained the 4s and 3d spectra of the samarium sample. The expected kinetic energy peaks according to the binding energies in [3] are presented in Table 3. We included the 1s energy for oxygen, as it is a transition that is likely to be observed due to the presence of oxygen in the surface of the Sm sample, for it had been not cleaned due to practical difficulties.

Level	Al source ($h\nu$=1483.6 eV)	Mg source ($h\nu$=1253.6 eV)
$3d_{3/2}, 3d_{5/2}$	375.5 eV, 403.2 eV	142.7 eV, 170.2 eV
$4s$	1122.9 eV, 1128.7 eV	900.3 eV, 906.1 eV
$1s$ (O)	949.6 eV	710.5 eV

Table 3: Literature values of the energy peaks expected for a (contaminated) Sm sample in XPS spectra for different X-ray sources. The 4s level is an energy doublet because we have considered the magnetic spin-spin exchange splitting. We have included a line for oxygen because the sample had not been cleaned for a long time.

4.3 Chemical analysis of a 10 DM coin

Lastly we have taken a spectrum of a 10 DM coin and tried to determine the unknown components. The 10 DM was minted out of silver and copper so we expected to find mainly this metals. The XPS measurement for this sample has been performed with the Al source.

5 Results

In this section we are going to present the photoemission spectra that were obtained for our different samples and different X-ray sources.

For the resolved spectra of the different peaks 'raw' data with their corresponding background can be consulted in Annex B at the end of this report. The backgrounds measured in this experiment have been fitted numerically to linear, quadratic or error functions depending on the case and have been subtracted from our experimental data for an optimal fit of our energy peaks.
For both samples we obtained first the full energy range spectrum and then we focused on different positions in the kinetic energy axis so we could see better the peaks and fit them.

5.1 Silver spectrum

For the silver sample, the following spectra were obtained. In Figure 4 we can see the full XPS spectrum of silver taken with the two aforementioned x-ray sources. The different features of the spectrum that we are going to look into in more depth are already visible here although from one curve to the other they are shifted as we represented the spectra referring to the kinetic energy of the photolectrons. Furthermore, we can see two rather intense features that appear at the same location for the two different incident kinetic energies. This fact lead us to identify them as Auger transitions, for the energy of the Auger electrons does not depend on the incident energy unlike the photoelectrons. The spectra represented for binding energies can be however consulted in Annex 1.

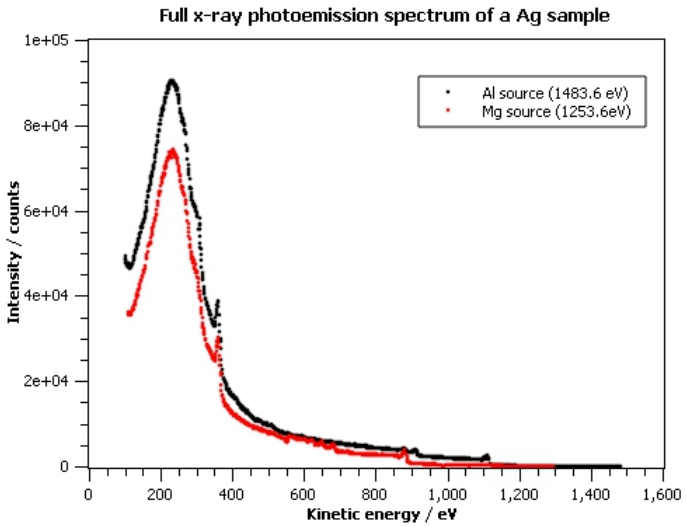

Figure 4: Full kinetic energy spectra for the Ag sample, plotted together for both X-ray sources.

In Figure 5 we can see the spectrum for the 3s-electrons photopeak of our silver sample. For the magnesium source, even if our set of data is not of great resolution and the number of counts is rather low we were able to fit the experimental points to a Gaussian peak with a linewidth of 7.9 $\pm$ 0.9 eV around the expected position. The exact position of the peak is written in Table 4. However, for the case of the aluminum source the data collected at the lab was utterly impossible to fit to any feature. The data corresponding to this measurement can be consulted in Figure 19 in Annex 2.

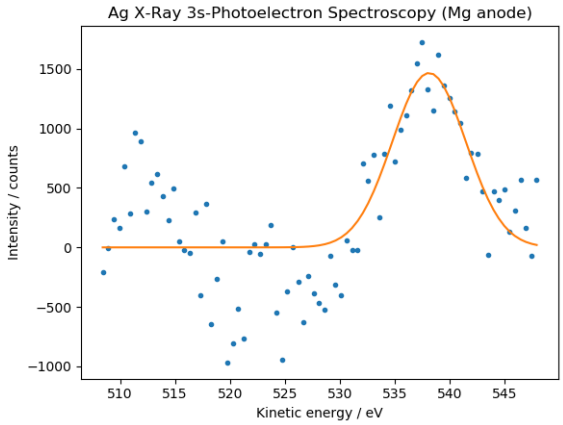

Figure 5: Silver 3s-level spectrum measured for the magnesium X-ray source. The results for the Al source did not give any visible peak, so we are not considering it. The experimental data were obtained using the parameters range = 510 eV - 550 eV, step = 0.5 eV, pass energy = 30 eV.

Our results for the pair of peaks corresponding to the photoelectrons from the 3p subshell of the silver atom were luckily more conclusive. In Figure 6 and Figure 7 we can see the resolved spectra for this energies. For both spectra taken with the two different sources two not overlapping peaks can be clearly observed. They were fitted to two Gaussians in the positions shown in Table 4 and with the bandwidths of 7.4 eV. Furthermore the ratio between their heights is 1.6 ± 0.1 and 1.75 ± 0.11 respectively for each source.

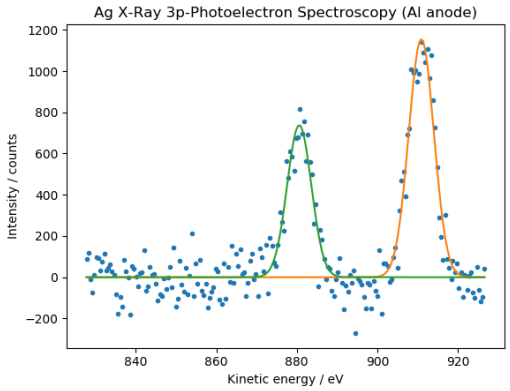

Figure 6: Silver spectrum for the 3p-levels measured with the magnesium source. The parameters for this measurement are range = 870 eV - 920 eV, step = 0.3 eV, pass energy = 30 eV.

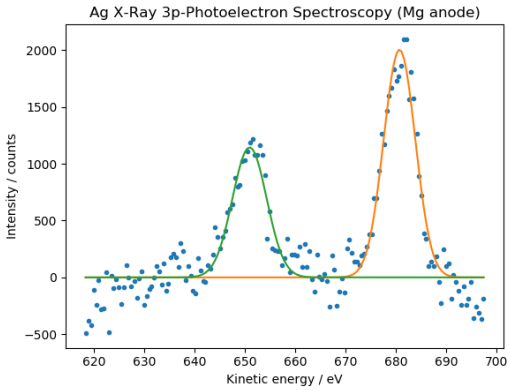

Figure 7: Silver 3p-spectrum taken for the aluminum source. Spectrum obtained using the parameters range = 620 eV - 700 eV, step = 0.5 eV, pass energy = 30 eV.

In Figure 8 and Figure 9 we can now see the energy spectra focused on the 3d peaks of silver. When trying to do the fitting of the peaks we observed that they did not have a symmetrical shape so the Gaussian function did not seem like the right choice. After some research we found that a fit into the sum of two Doniach-Sunjic [6] functions was the suited fit for this type of transitions. The location of the peaks of these functions are

shown in Table 4 and the ratio between their maxima of intensity resulted 1.3 ± 0.1 for both cases

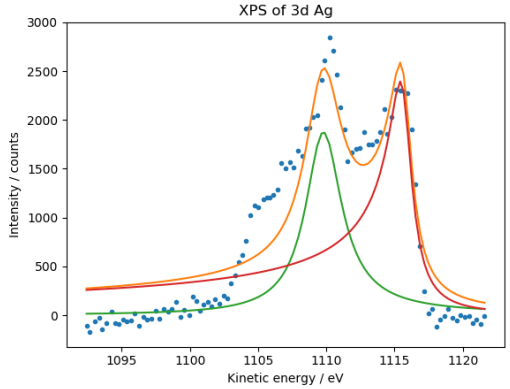

Figure 8: 3d-spectrum of silver for the aluminum X-ray source. The parameters that have been used are range = 1095 eV - 1125 eV, step = 0.3 eV, pass energy = 30 eV.

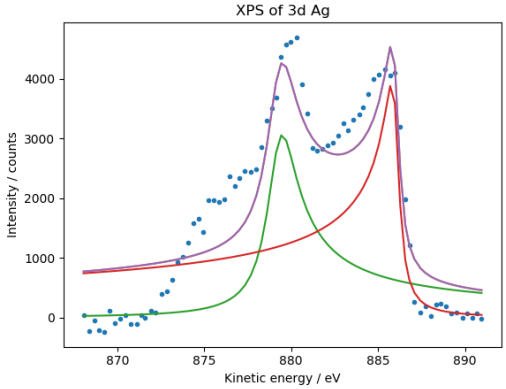

Figure 9: Spectrum with the 3d levels of silver, measured for an magnesium source. Obtained using the parameters range = 860 eV - 930 eV, step = 0.3 eV, pass energy = 30 eV.

5.2 Samarium spectrum

Afterwards we carried on the survey of the freshly evaporated samarium surface. The full spectrum of the sample is shown in Figure 12. Again we can see that the spectrum is dominated by a large peak located at the same position for both sources so the features we want to investigate need to be zoomed in.

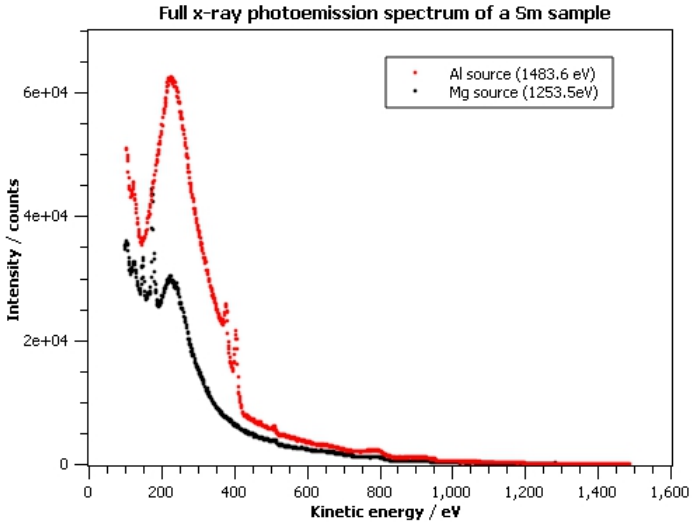

Figure 12: Kinetic energy spectra for the samarium sample and both aluminum and magnesium sources.

As it has already been commented, our spectrometer was calibrated for probing silver samples so in order to obtain the right values for the binding energies we had to first measure the Fermi edge of the sample and then refer our energies to this value. The following results presented in Figure 10 and Figure 11 are this

measurement of the Fermi level for the Sm sample.

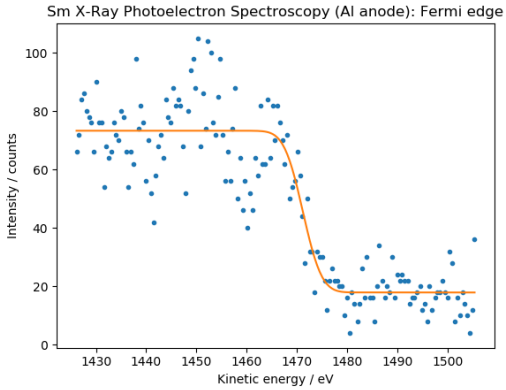

Figure 10: Fermi edge of the samarium spectrum measured with the aluminum source. Parameters used to obtain it: range = 1430 eV - 1510 eV, step = 0.5 eV, pass energy = 30 eV.

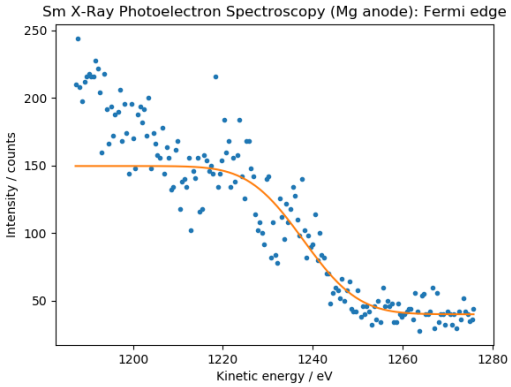

Figure 11: Fermi edge at the samarium spectrum for the magnesium X-ray source. Obtained using the parameters range = 1190 eV - 1280 eV, step = 0.5 eV, pass energy = 30 eV.

We fitted the edges to error functions, which allowed us to calculate the following values for the Fermi edges:

$$\begin{aligned} E_F^{Sm(Al)} &= (15.5 \pm 0.5)eV \\ E_F^{Sm(Mg)} &= (15.0 \pm 1.0)eV \end{aligned} \tag{6}$$

In Figures 13 and 14 we can see the samarium spectra focused on the energy range where we can observe the kinetic energies corresponding to the photoelectrons from the 3d levels. These peaks were fitted to a sum of Gaussian functions with bandwidths 5.3 ± 0.1 eV for the magnesium anode and 8.6 ± 0.2 eV for the aluminum one. The ratio between the heights of the two peaks of the same multiplet was 1.26 ± 0.03 eV for the measurements taken with the magnesium anode and 1.33 ± 0.02 eV for the ones taken with the aluminum anode. The positions are shown in Table 5.

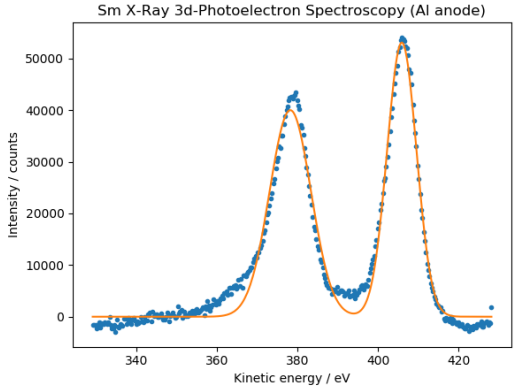

Figure 13: Spectrum of the samarium sample with the kinetic energies corresponding to the 3d levels for the aluminum source. Parameters used to obtain it: range = 330 eV - 430 eV, step = 0.3 eV, pass energy = 30 eV.

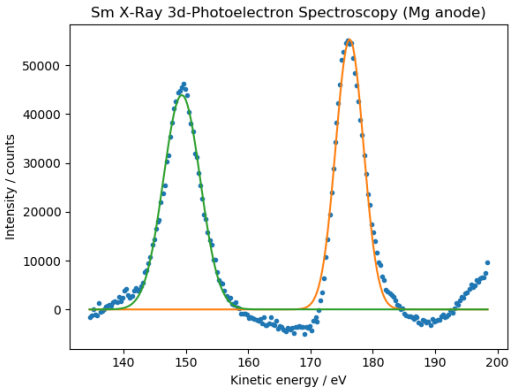

Figure 14: Samarium spectrum for the 3d levels measured with the magnesium source. Obtained with the parameters range = 135 eV - 200 eV, step = 0.3 eV, pass energy = 30 eV.

The 4s-levels of samarium photopeaks are shown in Figures 15 and 16. We can see in them that the results for the Al X-ray source gave us a wide peak instead of two distinguishable ones, we fitted it nevertheless to two Gaussians as that was what we expected to see because of the magnetic spin-spin exchange splitting.

For the Mg anode the splitting is easier to see, even if the amount of data collected was rather small.

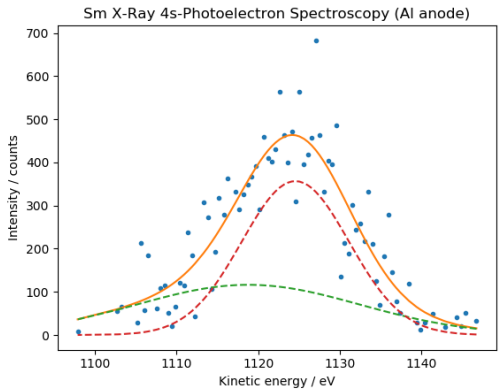

Figure 15: Sm spectrum for the energies corresponding to the 4s level for the Al anode. Obtained with the parameters range = 1100 eV - 1150 eV, step = 0.5 eV, pass energy = 30 eV.

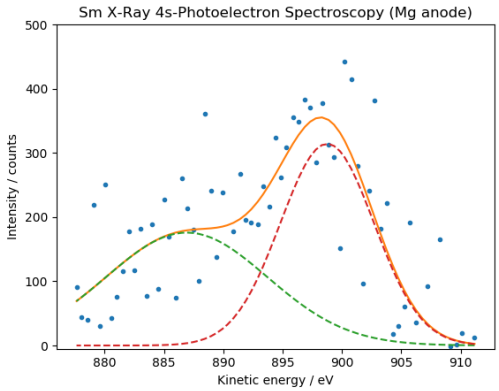

Figure 16: Sm spectrum with the energies of the 4s level, measured with the Mg X-ray source. The parameters that have been used to obtain this spectrum are range = 880 eV - 930 eV, step = 0.5 eV, pass energy = 30 eV.

Finally, kinetic energy peaks corresponding to the 1s-level of oxygen could also be observed in the samarium spectrum. They are shown in Figures 17 and 18. Both were fitted to two Gaussian functions with bandwidths 6.0 ± 0.3 eV for the case of the magnesium source and 7.6 ± 0.2 eV for the case of the aluminum one.

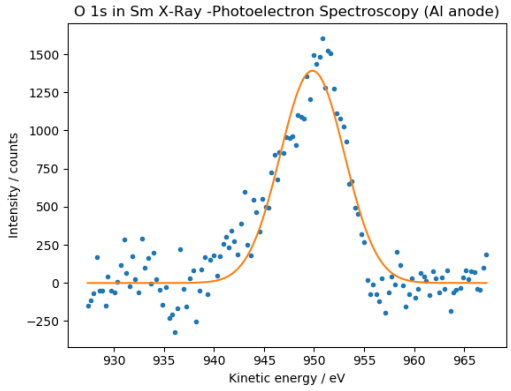

Figure 17: Presence of a 1s line in the Sm spectrum coming from oxygen, as the sample could not be cleaned. Spectrum measured with the Al anode. Obtained with the parameters range = 930 eV - 970 eV, step = 0.3 eV, pass energy = 30 eV.

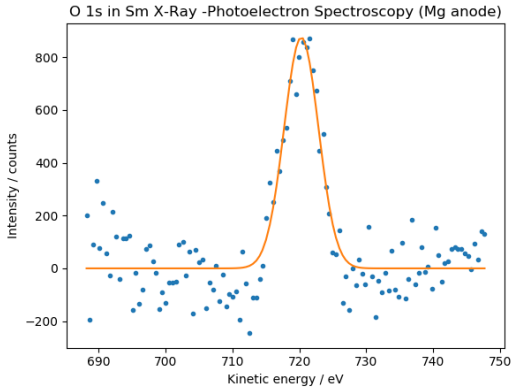

Figure 18: 1s energy peak coming from oxygen in the Sm spectrum. This result has been measured with the Mg X-ray source.Parameters used to obtain this result: range = 690 eV - 750 eV, step = 0.3 eV, pass energy = 30 eV.

5.3 Coin spectrum

Finally we probed our 10DM coin with the magnesium source. The main elements that we expected were not only silver and copper, but also other elements present in the air, as the coin has not been cleaned in a long time. In Figure 19 it is shown the full spectrum.

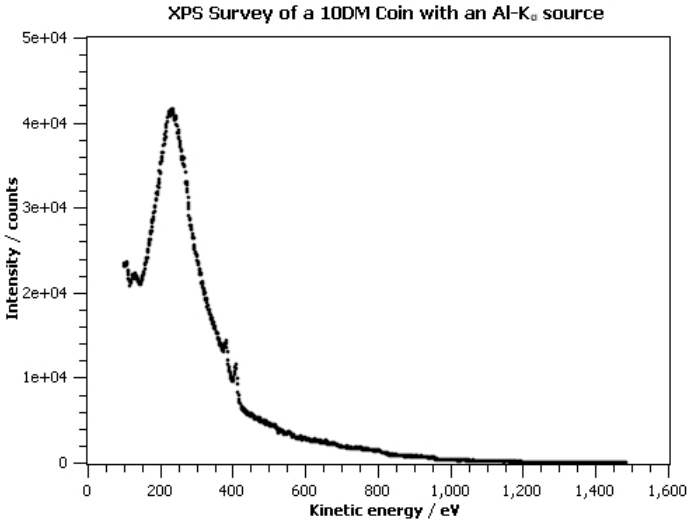

Figure 19: Full XPS kinetic energy spectrum for our coin sample, measured with an Al X-ray source.

Besides the large feature that we also encountered in the other spectra we selected two energy ranges where we found energy peaks and we measured two additional spectra: one at the energy range 450-600 eV and another for 840-1000 eV. These further spectra are shown in Figure 20 and Figure 21. We could identify up to five different peaks that were fitted to Gaussians. The position of the peaks of these features are shown and discussed in Table 6.

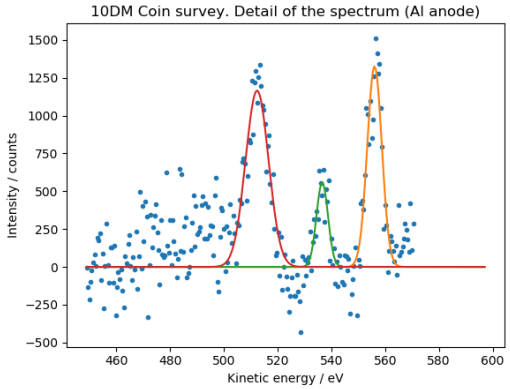

Figure 20: XPS spectrum for our sample of a 10DM coin in the kinetic energy range 450 eV - 600 eV.

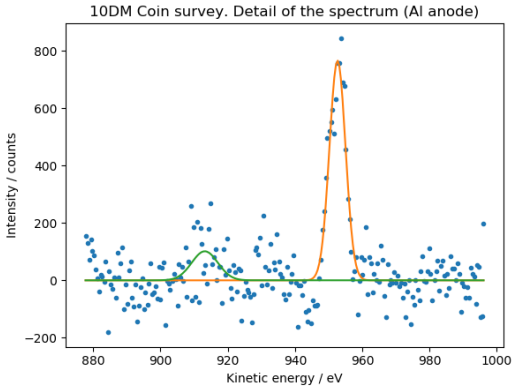

Figure 21: XPS spectrum for our sample of a 10DM coin in the kinetic energy range 840 eV - 1000 eV.

6 Discussion

In this section we will analyze the results that have been presented in the last section. After having obtained the experimental kinetic energies by fitting the peaks into Gaussian functions, we will be able to obtain the experimental binding energies that can be compared to the literature values [3][4].

6.1 Silver spectrum

Level	Al - E_B^{exp} (eV)	Mg - E_B^{exp} (eV)	E_B^{lit} (eV)
$3d_{3/2}$	376.9 ± 0.2	374.3 ± 0.2	374
$3d_{5/2}$	370.9 ± 0.1	367.6 ± 0.1	368
$3p_{1/2}$	606.0 ± 0.2	602.6 ± 0.2	603
$3p_{3/2}$	575.6 ± 0.1	572.8 ± 0.1	573
3s	-	715.5 ± 0.4	719

Table 4: Experimental vs. literature values of the Ag 3d, 3p and 3s binding energies for both Mg and Al sources [4]. Experimental values obtained by fitting the data plotted in Figures 5, 6, 7, 8 and 9.

The position of the center of our Gaussian fits to the 3p and 3s photopeaks, as well as the position of the maxima of our asymmetric function fit are shown in Table 4. Here we can also see the literature values for such features. The accordance of our experimental data with the literature values is quite satisfactory, given the difficulty of some of the fits. In particular for the case of the 3d peaks the fit to the asymmetric Doniaj-Sunic function seems to be rather effective for the purpose of correctly identifying the peaks and roughly describing the shape of the feature. The linewidth of these peaks was always around 7-8 eV. Knowing that the width of the incident radiation of our setup is less than 1 eV (see Table 1) and that the contribution of the electron energy analyzer is also about 1 eV the rest of it must come from thermal broadening. Finally regarding the ratio between the heights of the peaks for the theoretically expected relation of 2:3 is not too far from our experimental results of 1.4 for the 3d levels and 1.6 for the 3p ones. However here a better resolution could be achieved by improving the characterization of the background and the fitting, specially for the case of the asymmetric peaks.

6.2 Samarium spectrum

In Figures 10 and 11 we could observe the Fermi edges for both spectra of Sm using the two different X-ray sourced that we had. Those figures could be fitted relatively easily into error functions in which the Fermi edge is considered to be the point where the amplitude is half of its maximum value. The obtained values were:

$$\begin{aligned} E_f^{Sm(Al)} &= (15.5 \pm 0.5)eV \\ E_f^{Sm(Mg)} &= (15.7 \pm 1.0)eV \end{aligned} \tag{7}$$

Unfortunately we don't have any literature values to compare with, but the degree of agreement between our two experimental measurements make them likely to be correct.

Level	Al - E_B^{exp} (eV)	Mg - E_B^{exp} (eV)	E_B^{lit} (eV)
$3d_{3/2}$	1096.4 ± 0.6	1089.2 ± 1.1	1110.9
$3d_{5/2}$	1066.7 ± 0.8	1052.3 ± 1.1	1083.4
4s	353 ± 11	350 ± 4	353.3
4s	347 ± 1	338 ± 1	347.5
1s (O)	524.8 ± 0.6	518.3 ± 1.1	543.1

Table 5: Comparison between the obtained binding energies for the 4s and 3d levels of Sm and the corresponding literature values [4]. Experimental values come from the fitting of the spectra in Figures 13, 14, 15, 16, 17 and 18.

In Table 5 we can see the comparison of our measured energies for the different considered photopeaks of our samarium sample and the corresponding literature values. The agreement between the literature and the experiment results is good overall, even if one can notice that the spectrometer was calibrated for measurements with silver. Regarding the 3d-peaks the theoretical ratio of heights of 2:3 is here not reached (we get ratios of 1.33 and 1.26). We can again put the blame on the sometimes troublesome characterization of the background, for the fitting of the peaks seems to be suited.
In relation to the 4s spectrum the measurements using the aluminum X-ray source we could observe a rather faint splitting of the one peak to two due to the spin-spin exchange interaction. The effect was more visible for the data collected with the magnesium anode, despite the lower number of counts. Anyhow a deeper investigation would be needed to investigate the phenomenon of magnetic spin-spin exchange splitting in more depth.
Lastly, a peak of oxygen was found due to the lack of cleaning of the sheet of metal were the samarium was evaporated.

6.3 Coin spectrum

In Table 6 we can see the energies of the peaks found in the spectrum of the 10DM coin and our identification of their cause with the corresponding literature value of the energy that we have compared with.

Element	E^{exp} (eV)	E^{lit} (eV)	Type
Cu	947.0 ± 0.3	952.3	Binding energy ($2p_{3/2}$)
Cu	927.5 ± 0.4	932.7	Binding energy ($2p_{1/2}$)
Ag	570.4 ± 1.1	573.0	Binding energy ($2p_{3/2}$)
O	531.0 ± 0.1	543.1	Binding energy (1s)
Ag_2O	512.4 ± 0.3	513.2	Auger

Table 6: Characteristic energies and their corresponding elements for the coin XPS spectrum. Literature values are included for comparison, and have been taken from [4] [7]. Experimental values come from the fitting of the data plotted in Figures 20 and 21.

First of all we can see that the expected compounds of the coin, silver and copper, were identified. Moreover since as we have already said it was impossible for us to clean the coin, we could find again some oxygen characteristic energies in our results, apart from the copper and the silver which we knew were present in the coin. In summary, traces of copper, silver and oxygen were found.

7 Conclusions

In conclusion we have performed several experiments of x-ray photoelectron spectroscopy on two samples, silver and samarium, and thus we could probe their electronic structure measuring the peaks from the electrons removed from the different shells of their atoms. We could characterize this emission determining as well the linewidth and the ratio between the peaks for the cases where the spin orbit coupling originated two peaks. Once we had a deeper understanding of this spectroscopy technique we were able to identify the compounds of a 10DM coin by looking at its spectrum.

Annex A: Binding energy spectra

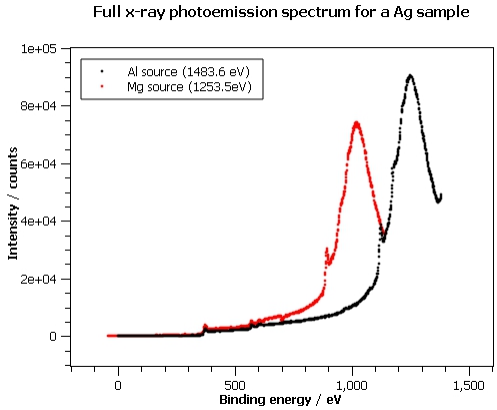

Figure 14: Complete binding energy spectra for the Ag sample, measured for both X-ray sources.

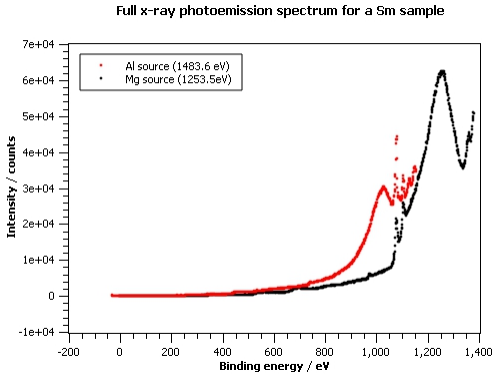

Figure 16: Full binding energy spectra for the Sm sample, plotted for both X-ray sources.

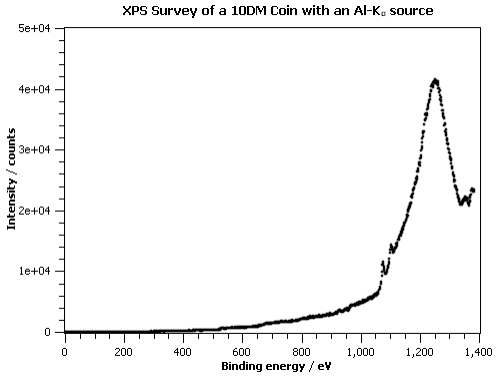

Figure 18: Complete binding energy spectrum for the coin sample, obtained from the kinetic energy one, shown in Figure 15.

Annex B: Background measurements

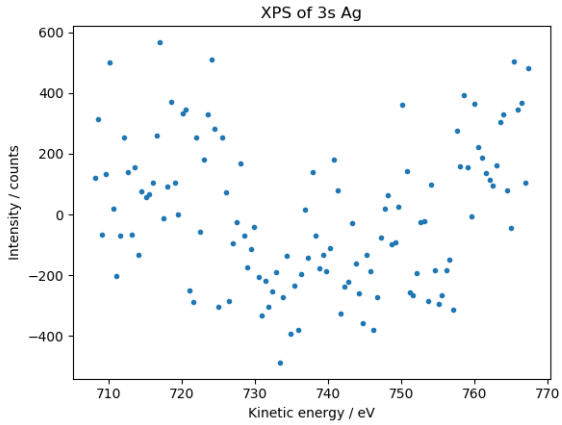

Figure 19: Ag 3s level spectrum for the Al source, with background.

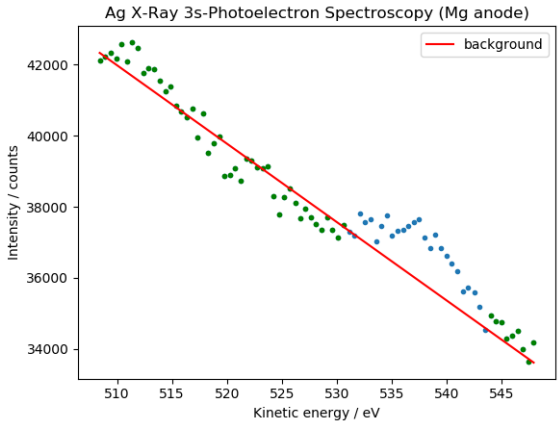

Figure 20: Ag 3s level spectrum for the Mg source.Nothing could be observed.

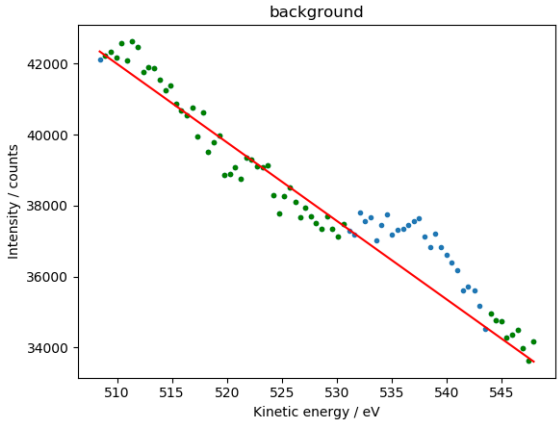

Figure 19: Ag 3s level spectrum for the Al source, with background.

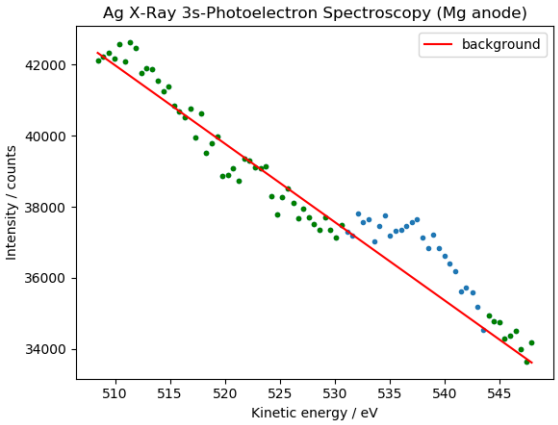

Figure 20: Ag 3s level spectrum for the Mg source, with background.

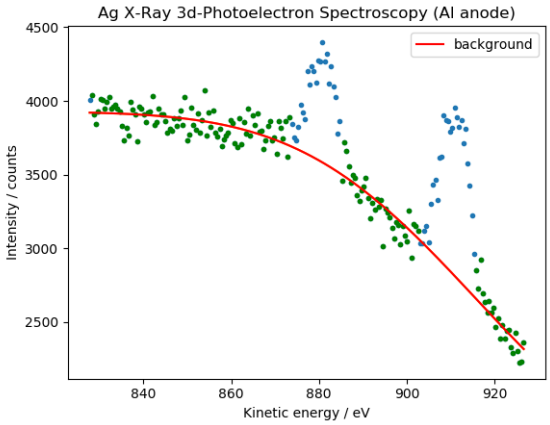

Figure 21: Spectrum with background radiation for the 3p levels of Ag, with the Al source.

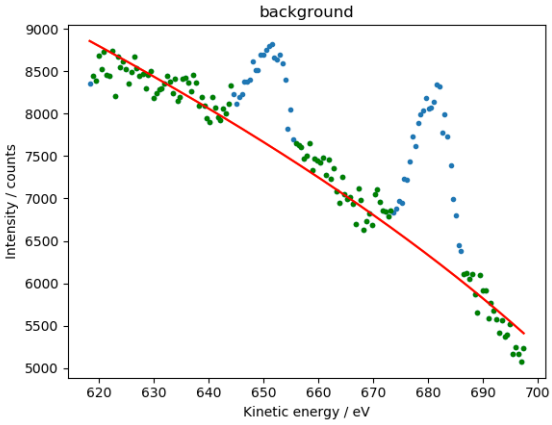

Figure 22: Spectrum with background radiation for the 3p levels of Ag, with the Mg source.

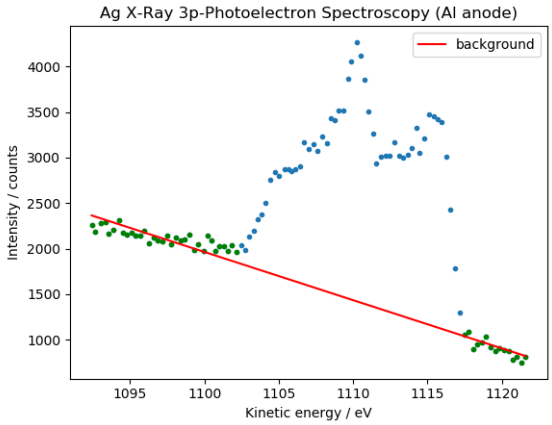

Figure 23: 3d Ag spectrum, with the Al source, considering background radiation.

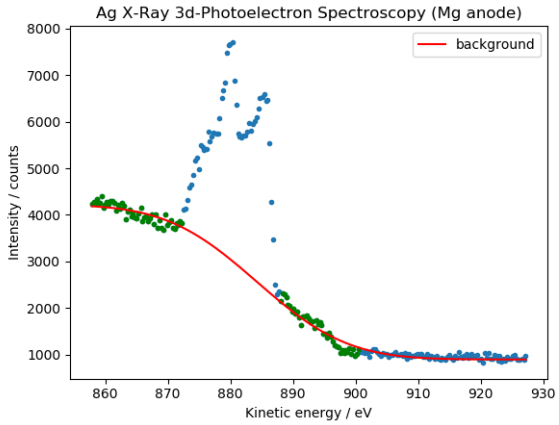

Figure 24: 3d Ag spectrum, with the Mg source, considering background radiation.

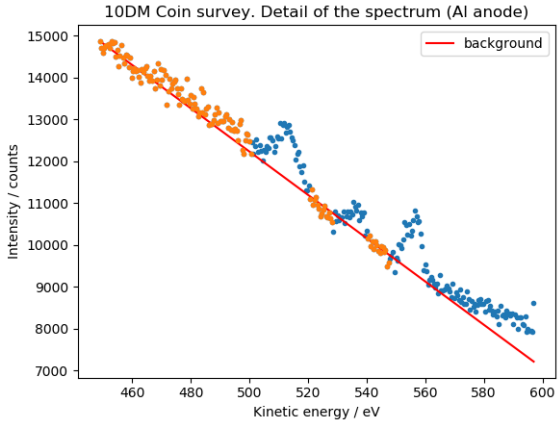

Figure 24: First energy range for the coin XPS spectrum, with background.

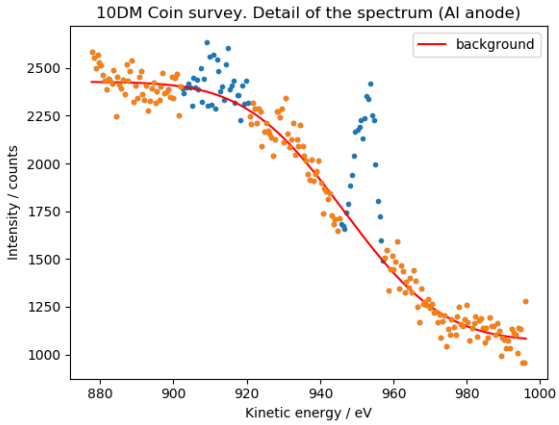

Figure 25: Second energy range for the coin XPS spectrum, with background.

References

[1] The introduction and tasks of XPS experiment, ttps://wiki.physik.fu-berlin.de/fp/lib/exe/fetch.php?media=private:xps-info-eng.pdf

[2] Rudy Schlaf, Calibration of Photoemission Spectra and Work Function Determination, http://rsl.eng.usf.edu/Documents/Tutorials/PEScalibration.pdf

[3] The tables of binding energies for various elements, https://wiki.physik.fu-berlin.de/fp/lib/exe/fetch.php?media=private:xps-bindingenergytable.pdf

[4] Electron Binding Energy Table - X-Ray Data Booklet, http://xdb.lbl.gov/Section1/Table1-1.pdf

[5] P.W. Palmberg, G.E. Riach, R.E. Weber, and N.C. Macdonald, Handbook of Auger Electron Spectroscopy, published by Physical Electronics Industries Inc.; NIST X-ray Photoelectron Spectroscopy Database, http://srdata.nist.gov/xps/

[6] Line Shapes, http://casaxps.com/help-manual/line-shapes.htm

[7] NIST XPS Database, https://srdata.nist.gov/xps/EnergyTypeValSrch.aspx